AGU PUBLICATIONS

Geophysical Research Letters

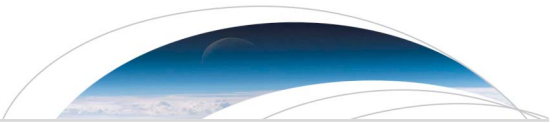

RESEARCH LETTER

10.1002/2015GL064443

Key Points:
- A long-term water vapor simulation with a chemical transport model
- Tropical water vapor response to stratospheric major warming
- The contribution to decadal changes of stratospheric water vapor

Supporting Information:
- Texts S1 and S2
- Figure S1
- Figure S2
- Figure S3

Correspondence to:
M. Tao,
m.tao@fz-juelich.de

Citation:
Tao, M., P. Konopka, F. Ploeger, M. Riese, R. Müller, and C. M. Volk (2015), Impact of stratospheric major warmings and the quasi-biennial oscillation on the variability of stratospheric water vapor, *Geophys. Res. Lett., 42*, 4599–4607, doi:10.1002/2015GL064443.

Received 4 MAY 2015
Accepted 8 MAY 2015
Accepted article online 13 MAY 2015
Published online 3 JUN 2015

Impact of stratospheric major warmings and the quasi-biennial oscillation on the variability of stratospheric water vapor

Mengchu Tao[1], Paul Konopka[1], Felix Ploeger[1], Martin Riese[1], Rolf Müller[1], and C. Michael Volk[2]

[1]IEK-7: Stratosphere, Forschungszentrum Jülich, Jülich, Germany, [2]Department of Physics, University of Wuppertal, Wuppertal, Germany

Abstract Based on simulations with the Chemical Lagrangian Model of the Stratosphere for the 1979–2013 period, driven by the European Centre for Medium-Range Weather Forecasts ERA-Interim reanalysis, we analyze the impact of the quasi-biennial oscillation (QBO) and of Major Stratospheric Warmings (MWs) on the amount of water vapor entering the stratosphere during boreal winter. The amplitude of H_2O variation related to the QBO amounts to 0.5 ppmv. The additional effect of MWs reaches its maximum about 2–4 weeks after the central date of the MW and strongly depends on the QBO phase. Whereas during the easterly QBO phase there is a pronounced drying of about 0.3 ppmv about 3 weeks after the MW, the impact of the MW during the westerly QBO phase is smaller (about 0.2 ppmv) and more diffusely spread over time. We suggest that the MW-associated enhanced dehydration combined with a higher frequency of MWs after the year 2000 may have contributed to the lower stratospheric water vapor after 2000.

1. Introduction

As first suggested by *Brewer* [1949], water vapor enters the stratosphere through the cold tropical tropopause layer (TTL) where freeze drying causes strong dehydration from large tropospheric to very low stratospheric mixing ratios [e.g., *Randel and Jensen*, 2013]. The variability of stratospheric water vapor has received considerable attention because of its key impact on the radiation budget and hence on surface climate [*Solomon et al.*, 2010; *Dessler et al.*, 2013]. The stratospheric water vapor entry values derived from almost three decades of satellite observations follow roughly the evolution of tropical tropopause temperatures and show multi-timescale variations ranging from daily to decadal [*Fueglistaler and Haynes*, 2005; *Fueglistaler et al.*, 2013; *Urban et al.*, 2014; *Hegglin et al.*, 2014].

Rosenlof et al. [2001] suggested that water vapor in the lower stratosphere may have increased by 1% per year in the second half of the 20th century. Less than 30% of this increase could be explained by oxidation of increasing methane concentrations [*Rohs et al.*, 2006; *Riese et al.*, 2006]. Further, observations over the last several decades indicate a strong interannual variability of lower stratospheric H_2O [*Oltmans et al.*, 2000; *Hurst et al.*, 2011; *Kunz et al.*, 2013]. Both satellite limb measurements by the Halogen Occultation Experiment (HALOE) and balloon-borne measurements over Boulder revealed a decrease in stratospheric water vapor since the end of 2000, consistent with a stronger tropical upwelling and lower temperatures in the TTL [*Randel et al.*, 2006; *Bönisch et al.*, 2011]. Recently, *Urban et al.* [2014] reported another drop in water vapor observations by the Aura Microwave Limb Sounder (MLS) onboard the AURA satellite, which happened after 2012, sharing similarity with the earlier drop around 2000.

However, the most pronounced signature of water vapor variations in the tropical lower stratosphere is the tape recorder effect [*Mote et al.*, 1996] reflecting the seasonal cycle of tropical tropopause temperatures. This annual cycle signal imprinted on the stratospheric water vapor mixing ratios at the tropical tropopause ascends with the Brewer-Dobson circulation (BDC). Beyond this annual cycle, the interannual variability is mainly influenced by the quasi-biennial oscillation (QBO, mean period of 28 to 29 months) [*Baldwin et al.*, 2001; *Dessler et al.*, 2013] and to a weaker extent by the El Niño–Southern Oscillation (ENSO) [*Randel et al.*, 2004; *Calvo et al.*, 2010]. In addition to these almost periodic components, transient, subseasonal cooling episodes occur at time scales of 1–2 months as a result of forcing by extratropical waves [*Randel et al.*, 2002].

As recently discussed by *Gómez-Escolar et al.* [2014] and *Tao et al.* [2015], this subseasonal variability of minimum temperatures in the tropical lower stratosphere follows the Major Sudden Stratospheric Warmings

(MWs). These extreme events not only warm the polar cap within a few days [e.g., *Andrews et al.*, 1987] but also affect the BDC. Thus, warming and intensified downwelling over the polar cap is accompanied by cooling and enhanced upwelling in the tropical stratosphere [e.g., *Holton et al.*, 1995].

Gómez-Escolar et al. [2014] further showed that this effect is strongly modulated by the QBO. At altitudes above ~40 hPa, tropical temperature anomalies associated with MWs persist longer during the westerly QBO phase (wQBO) than during the easterly QBO phase (eQBO). Conversely, below this altitude, enhanced cooling occurs only during the eQBO phase.

Although many studies focus on stratospheric water vapor trends, the subseasonal variability of water vapor still lacks quantitative attribution to the processes mentioned above. In this paper we utilize long-term model simulations to (1) quantify changes in stratospheric water vapor values related to MWs, (2) explain the mechanism in relation to different QBO phases, and (3) discuss possible links to decadal changes of stratospheric water vapor.

2. Major Stratospheric Sudden Warmings and the QBO

Based on ERA-Interim reanalysis and using the methodology presented by *Charlton and Polvani* [2007] (CP07 from now on), we identify 23 MWs from 1979 to 2013 (final warmings are excluded). The corresponding central dates, the first day when zonal wind reversed at 60°N and 10 hPa, are listed in Table 1 (second column). As has been pointed out [*Taguchi*, 2011; *Gómez-Escolar et al.*, 2014], use of the highest polar cap temperature instead of the zonal wind reversal at 60°N and 10 hPa, characterizes the response of the BDC to MWs better. Thus, in our study the MW central dates (Table 1, third column) are defined as the dates with highest mean polar cap temperature (60–90°N) within a ±30 day window around each MW central date derived from the wind criterion (CP07).

The QBO phase for each MW is defined using the 30 day smoothed equatorial mean wind at $\theta = 500$ K (approximately 50 hPa) calculated for each temperature-based central date. MWs with equatorial mean wind at 500 K less than ±5 m/s have occurred in the transition regime between two QBO phases and are excluded in the following statistical analysis (the corresponding central dates are shown in Table 1). The dates 21 February and 16 January are the average MW central dates in eQBO and in wQBO phase, respectively. These two dates will be used in the following statistical analysis as the central dates for the years without occurrence of MWs in the corresponding QBO phases.

3. Variability of Water Vapor in the Tropical Lower Stratosphere in Relation to MWs

One of the difficulties in quantifying the variability of stratospheric water vapor arises from limitations of the observational systems, especially due to issues arising from instrument drifts and short overlap periods. As recently discussed by *Hegglin et al.* [2014], chemistry-climate models nudged to observed meteorology have the potential to address these problems by providing a more homogeneous long-term data set.

As shown in Figure 1, we established a long-term water vapor data set from 1979 to 2013 using the Chemical Lagrangian Model of the Stratosphere (CLaMS) [*McKenna et al.*, 2002; *Konopka et al.*, 2004; *Pommrich et al.*, 2014]. Temperatures, horizontal winds, and diabatic heating rates are prescribed from the European Centre for Medium-Range Weather Forecasts (ECMWF) ERA-Interim reanalysis [*Dee et al.*, 2011]. The transport in CLaMS is based on 3-D forward trajectories and an additional small-scale mixing parameterization, which are sensitive to the deformation in the large-scale flow [*Konopka et al.*, 2004]. Methane oxidation is included as a source for water vapor in the middle and upper stratosphere, with the concentration of hydroxyl, atomic oxygen, and chlorine radicals taken from a model climatology [*Pommrich et al.*, 2014].

The lower boundary for the water vapor mixing ratio calculation is located at approximately 500 hPa and is set to the ERA-Interim water vapor field. The calculation of water vapor mixing ratios is based on a simplified dehydration scheme. If saturation (with respect to ice) occurs along a CLaMS air parcel trajectory, the water vapor amount in excess of the saturation mixing ratio is instantaneously transformed to the ice phase and sediments out, using a parameterization based on a mean ice particle radius and the corresponding fall speed [*Hobe et al.*, 2011; *Ploeger et al.*, 2013]. Furthermore, if the parcel is subsaturated and ice exists, this ice is instantaneously evaporated until saturation is reached.

The CLaMS tropical zonal mean (10°S–10°N) deseasonalized water vapor and diabatic vertical velocity $\dot{\theta}$ anomaly (relative to the 35 year climatology, black lines in Figures 1 (top) and 1 (bottom), respectively) at

Table 1. Central Dates of the MWs in eQBO and wQBO Phases[a]

No.	MWs Central Date (Wind)	MWs Central Date (Temp)	MW Magnitude ΔT_{10} (K)
		wQBO	
1	22 Feb 1979	27 Feb 1979	5.9
2	4 Mar 1981	5 Feb 1981	13.7
3	14 Mar 1988	12 Mar 1988	13.6
4	21 Feb 1989	20 Feb 1989	12.3
5	20 Mar 2000	13 Mar 2000	10.4
6	18 Jan 2003	29 Dec 2002	13.1
7	24 Feb 2007	24 Feb 2007	3.3
8	24 Jan 2009	23 Jan 2009	14.4
	24 Feb 1984[b]	24 Feb 1984[b]	12.3
	8 Dec 1987[b]	8 Dec 1987[b]	12.1
Average	21 Feb	15 Feb	10.8 ± 4
		eQBO	
1	1 Mar 1980	1 Mar 1980	14.2
2	1 Jan 1985	1 Jan 1985	12.5
3	15 Dec 1998	17 Dec 1998	13.1
4	30 Dec 2001	28 Dec 2001	16.0
5	5 Jan 2004	25 Dec 2003	12.5
6	21 Jan 2006	21 Jan 2006	7.7
7	22 Feb 2008	23 Feb 2008	5.9
8	6 Jan 2013	11 Jan 2013	11.6
	23 Jan 1987[b]	18 Jan 1987[b]	7.7
	26 Feb 1999[b]	27 Feb 1999[b]	12.5
	11 Feb 2001[b]	1 Feb 2001[b]	4.8
	17 Feb 2002[b]	19 Feb 2002[b]	4.0
	9 Feb 2010[b]	30 Jan 2010[b]	11.4
Average	16 Jan	16 Jan	11.7 ± 3

[a]The second column shows the central dates according to the wind reversal criterion of *Charlton and Polvani* [2007]. The third column shows the central dates according to the maximum polar cap temperature [*Taguchi*, 2011]. The QBO phase is defined by 30 day smoothed equatorial mean wind at $\theta = 500$ K (~50 hPa).

[b]The MWs within the transition regime between two QBO phases. The magnitudes of MWs in the fourth column are estimated from the polar cap (50°N–90°N) temperature anomaly at 10 hPa averaged over ±5 days around the temperature-based central date.

400 K (~18 km), show a clear negative correlation ($r = -0.6$). We find a very good agreement between the simulation and the Microwave Limb Sounder (MLS) measurements onboard the Aura satellite (purple line in Figure 1). Also with the observations of the Halogen Occultation Experiment (HALOE, green) on board the Upper Atmosphere Research Satellite, the simulation shows good agreement. The good agreement between HALOE observations and the simulation is better after 2000 than before. Before 2000, the relatively low simulated water vapor values compared with HALOE are consistent with a low bias of tropical tropopause temperature in ECMWF reanalysis data [*Dee et al.*, 2011], which has been corrected in 2006 after including new satellite data (COSMIC) into the 4D-Var assimilation procedure [*Fueglistaler et al.*, 2013]. Note that the water vapor drops around 2000, and 2012 observable in the satellite data are also reflected in the CLaMS simulation.

The MWs in boreal winter occurred mostly in January and February and are marked in Figure 1 as the vertical straight lines (MWs in the wQBO phase are colored in blue and those in the eQBO phase in red). Remarkably, many of the water vapor drops follow the MWs and the mean tropical upwelling (Figure 1, bottom) increases

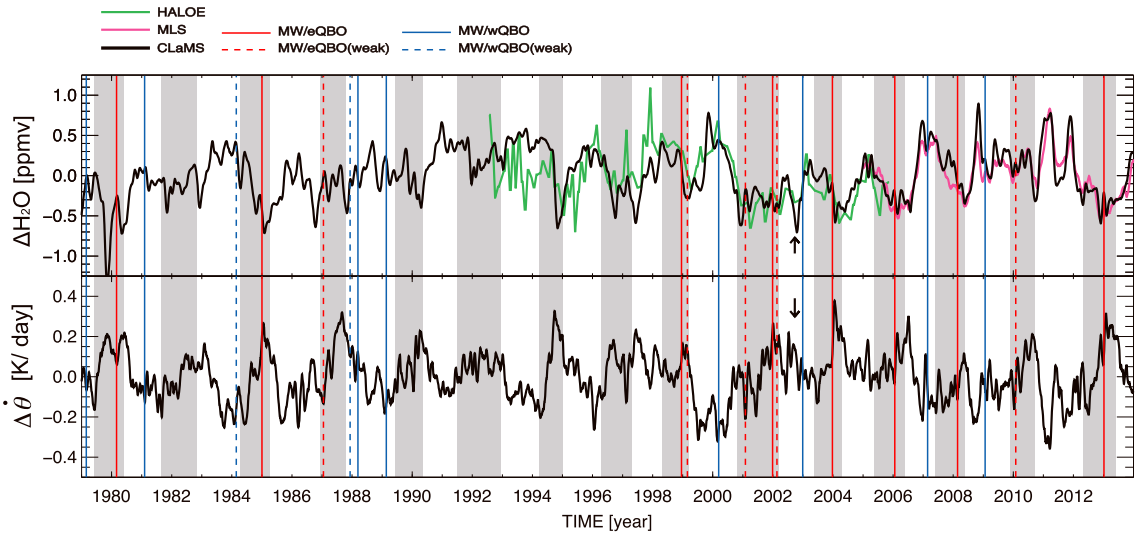

Figure 1. The evolution of (top) water vapor volume mixing ratios and (bottom) the ERA-Interim diabatic vertical velocities $\dot{\theta}$ in the tropics (10°S–10°N) at the 400 K potential temperature level (~18 km), shown as the deseasonalized anomaly with respect to the 35 year climatology. The black line shows the H_2O simulation from the CLaMS 35 year run; the green line shows HALOE; the purple line shows MLS satellite observations. A 15 day running mean is applied to all three data sets. The gray shadings highlight the QBO easterly phases (eQBO), which are defined by the ERA-Interim wind at 500 K (about 50 hPa). The vertical straight lines mark the central days of MWs: red during the eQBO, blue during the wQBO, and dashed lines are MWs with a weak QBO (QBO index less than ±5 m/s). The black arrow shows the position of the only MW in the Southern Hemisphere, which occurred in October 2002.

almost simultaneously. These characteristic drops in tropical water vapor usually happened 2–4 weeks after the central MW days and, notably, all these H_2O drops approximately coincide with most of the lowest water vapor anomalies during the considered 35 years except for the three lowest values in the mid-1990s.

3.1. The Tape Recorder Signal and QBO

Figure 2 provides the vertical structure of the tape recorder as observed by MLS (Figure 2a) and simulated with CLaMS (Figure 2b). The figure shows tropical zonal mean water vapor (10°S–10°N) with the time axis confined to boreal winter (DJF; December-January-February). We focus on boreal winter, because the MWs all happened in the Northern Hemisphere with the exception of one in the Southern Hemisphere in October 2002 (black arrow in Figure 1; this MW will be excluded from further discussion). A good agreement is achieved in terms of mean vertical structure and the slow upward phase propagation. However, the layer with the lowest water vapor mixing ratios around the tropopause is ~10 K higher in the CLaMS simulation than in the MLS observations. Furthermore, a faster upward propagation of the tape recorder signal is found above 430 K in CLaMS simulations. This excessive tropical upwelling is consistent with the temperature low bias in the ERA-Interim forecast [*Dee et al.*, 2011].

To quantify the effect of the QBO phase on the amount of water vapor entering the stratosphere, the vertical structure of the tape recorder derived from a 35 year CLaMS climatology is divided into two composites containing either years with eQBO or with wQBO phase (Figures 2c and 2d). In the 35 years, there are 18 boreal winters with wQBO phase and 15 winters with eQBO phase. Note that both the MLS and HALOE data sets are too short to make this type of analysis statistically significant. Similar as in Figures 2a and 2b, the tape recorder signal is seen in both QBO phases. However, obvious differences related to the QBO phase exist: First, the H_2O minimum between 380 and 420 K, resulting from intensive dehydration at the tropical tropopause during winter, is by ~0.5 ppmv lower during the eQBO than during the wQBO phase. Second, the tropical upwelling as represented in the H_2O tape recorder is faster for the eQBO years than for the wQBO years. All these impacts of the QBO phase on the tropical H_2O are consistent with previous studies [see, e.g., *Baldwin et al.*, 2001].

3.2. Net Effect of MWs

Because the annual cycle is the dominant feature of water vapor entering the tropical stratosphere, we consider in the following the deseasonalized anomalies (i.e., relative to the 35 year mean) of H_2O and temperature. Besides, we categorize the eQBO (wQBO) winters into eQBO (wQBO) winters with and without occurrence of MWs (eQBO/MW, wQBO/MW, eQBO/noMW, and wQBO/noMW). The composites of the deseasonalized anomalies of H_2O (colored) and temperature (gray contours) according to these categories are shown in

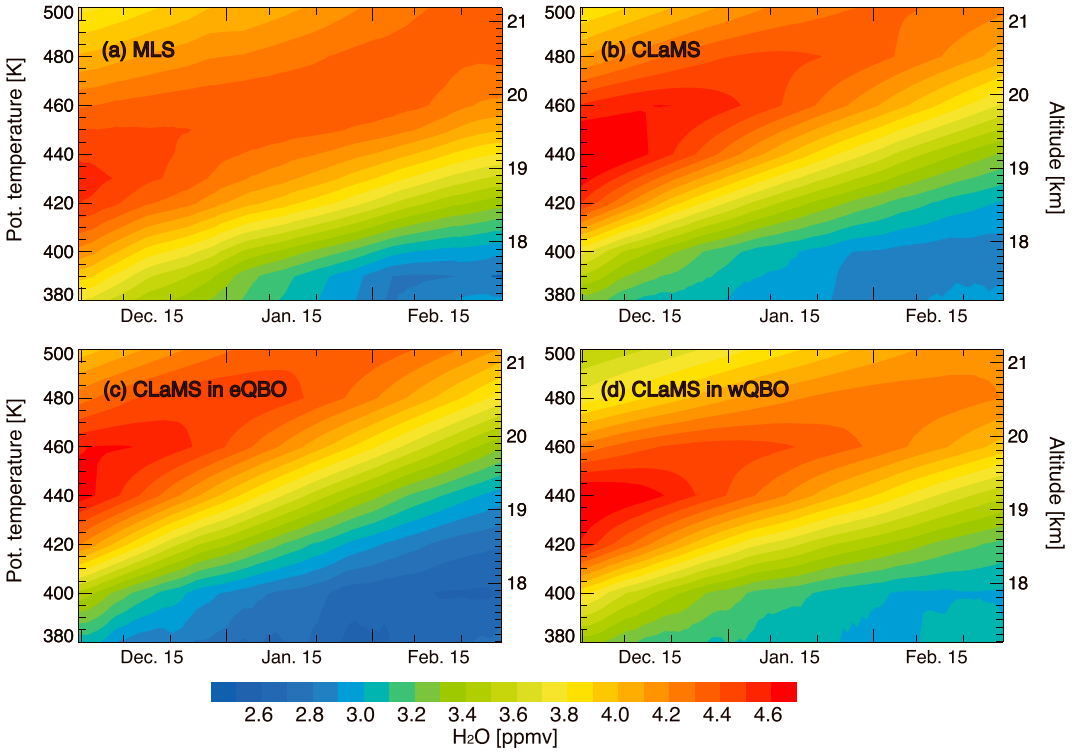

Figure 2. Tropical water vapor climatology (10°S–10°N, 2005–2013) during boreal winter (DJF) for (a) MLS observations and (b) CLaMS simulation. The same is shown for (c) eQBO phase composites and (d) wQBO phase composites, from CLaMS. Note that the averaging kernels of MLS are applied to CLaMS simulation Figure 2b for better comparison.

Figures 3a1 (eQBO/noMW), 3a2 (wQBO/noMW), 3b1 (eQBO/MW), and 3b2 (wQBO/MW). For years with MWs, ±90 day periods around each MW central date (as shown in Table 1) are used for composites. Note that the mean central date of wQBO/MW (15 February) is 1 month later than that of eQBO/MW (16 January). Considering the time shift of MW relative to the QBO phase, the composite for eQBO/noMW (wQBO/noMW) cases is centered at 16 January (15 February) with a ±90 day window. To separate the MW effect from the QBO variability, we composite the differences between eQBO/MW (Figure 3b1) and eQBO/noMW (Figures 3a1 and 3c1) estimating the MW net effect in the eQBO phase (analogously for wQBO in Figure 3c2).

First, the eQBO case is colder (~1.5 K) and drier (~0.5 ppmv) in the lower stratosphere compared with the wQBO case, independent of the MW occurrence (cf. Figure 3a1 with Figure 3a2 for winters without MW and Figure 3b1 with Figure 3b2 for winters with MW). Beyond the upward propagating anomaly branch starting in early winter (white arrows), a fast upward propagating branch with low H_2O anomaly values (green arrows) can be diagnosed in both QBO phases during MW (Figures 3b1 and 3b2). The upward propagating low H_2O anomaly can be better seen if it is separated from the QBO variability (Figures 3c1 and 3c2). These subseasonal signatures start at $\theta = 380$ K about 15–30 days after the (mean) central day and propagate up to 480 and 420 K in the eQBO and wQBO phase in the following 1–2 months. Furthermore, both of these subseasonal negative H_2O anomalies are accompanied by drops of the tropical temperature (gray dashed contours). However, the tropical cooling in the eQBO is the strongest (up to 2 K anomaly) at 430 K about 15 days after the MW onset and reduces the tropopause temperature by approximately 1 K. The cooling for wQBO/MW (Figure 3c2) weakens below about 450 K and the negative temperature anomaly almost disappears when reaching the tropical tropopause. This asymmetric response of tropical temperature relative to the QBO phase is consistent with the results discussed by *Gómez-Escolar et al.* [2014] (see also next section).

It is shown in Figures 3c1 and 3c2 that H_2O differences are below 0.2 ppmv and without statistical significance before the MW central date. The direct dehydration following the MWs (after the central date) is evident for both QBO phases (green arrows in Figures 3c1 and 3c2). There is a drop of water vapor (0.2–0.3 ppmv) around

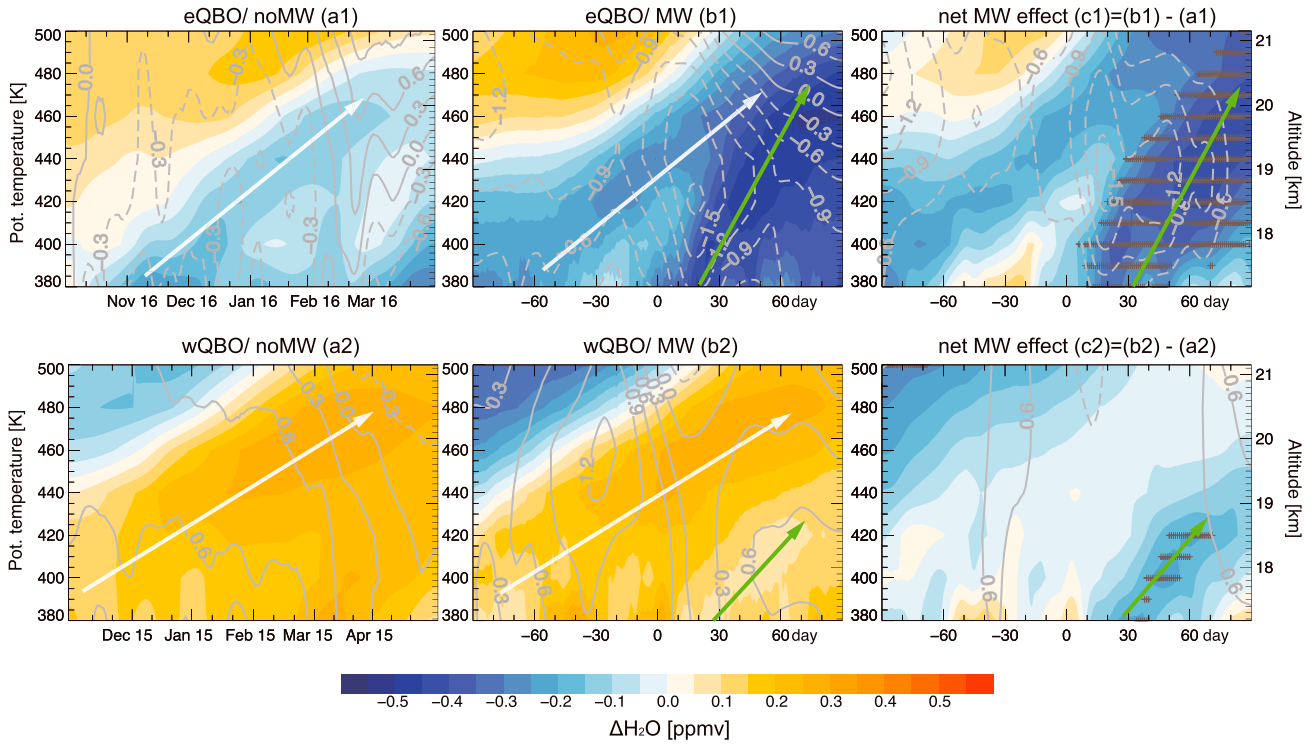

Figure 3. Composites of CLaMS tropical (10°S–10°N) deseasonalized anomaly for water vapor (colored) and temperature (gray contours, solid/dashed for positive/negative values) for (top row) eQBO and (bottom row) wQBO composites. (a1 and a2) All the boreal winters without MWs. (b1 and b2) The winters with MWs within a ±90 day window around each MW are collected. (c1 and c2) The respective differences, i.e., (b1) − (c1) and (b2) − (c2) show the net effect of the MWs during the eQBO and wQBO, respectively. Note that in the years without an MW event, the mean central dates of MW/eQBO (16 January) and MW/wQBO (15 February) cases are used. Crosses denote ΔH_2O results with statistical confidence above 0.9 (Monte Carlo difference test).

the tropopause 15–30 days after the MW central day, which results from TTL cooling after the MW onset, shown by the temperature differences (gray contours) due to MWs in Figures 3c1 and 3c2. Both responses pass the Monte Carlo difference test (see supporting information) at 0.9 confidence level (crosses). The anomalies propagate upward and strengthen by ~1 ppmv. The enhancement of upward propagating anomalies are related to the dilution rate of tropical air by midlatitude air through horizontal transport and diffusion (termed inmixing) that is of importance to water vapor tape recorder in lower stratosphere [*Mote et al.*, 1998]. The ascending anomaly increases more strongly (and steeper) during eQBO. It is mainly because of the faster upward transport and consequent less inmixing from midlatitude air during the easterly phase.

Another important difference is related to the QBO phase: The MW-related cooling and subsequent dehydration during the eQBO phase can be well separated from the change of the background and contributes to about ~0.3 ppmv H_2O drop about 2–4 weeks after the central date of the MW. On the other hand, a much smaller decrease of H_2O relative to the background about ~0.1 ppmv can be diagnosed during the wQBO phase. Note that the mean strength of MWs in 2 QBO phases do not differ much, less than 10% (see the fourth column of Table 1). That means the strength of MWs in different QBO phases cannot explain the different responses of tropical water vapor to MW.

3.3. MWs, BDC, and the QBO-Dependent Dynamical Background

The extratropical planetary waves in the stratosphere intensify during the weeks directly preceding the MWs [*Limpasuvan et al.*, 2004]. This upper stratospheric wave breaking triggers the MWs and accelerates the deep branch of the BDC [e.g., *Holton et al.*, 1995]. The enhanced wave breaking results in enhanced polar downwelling, enhanced tropical upwelling, and increased cooling in the tropical stratosphere. The wave forcing during MWs intensifies not only in high latitudes but also in the subtropical lower stratosphere. The related subtropical wave driving can be a result of modified wave-propogation conditions (lower stratospheric zonal mean wind) [*Garcia and Randel*, 2008] or because waves are generated by deep convection in the tropics and subtropics [*Kerr-Munslow and Norton*, 2006; *Norton*, 2006; *Chen and Sun*, 2011].

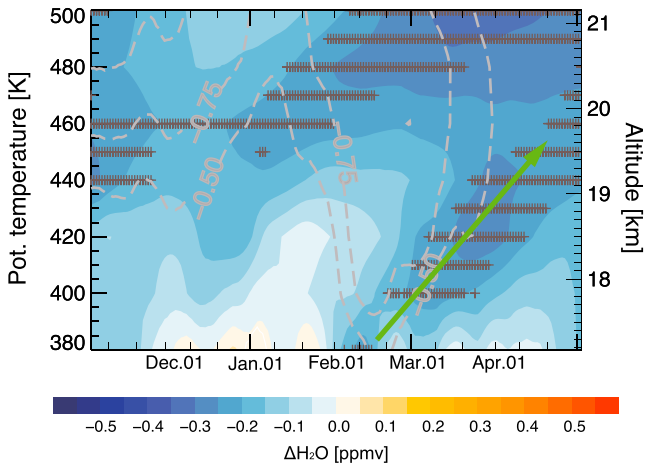

Figure 4. Differences of tropical (10°S–10°N) water vapor (colored) and temperature (gray contours) deseasonalized anomalies derived from the 35 year CLaMS simulation between winters in the 2000s and winters in the 1990s (2000s minus 1990s). Gray crosses indicate statistical confidence larger than 0.9 as derived from the Monte Carlo test.

The wave dissipation at low latitudes is modulated by the QBO-related zero-wind line. During the eQBO phase, the zero-wind line is much lower (around 30 hPa) than during wQBO phase (around 10 hPa). Hence, the low-latitude wave dissipation occurs at lower levels during eQBO winters and efficiently accelerates the shallow branch of the BDC [*Garny et al.*, 2011; *Gómez-Escolar et al.*, 2014].

Therefore, drops of tropical temperature in the lower stratosphere are expected during winters with MWs in both QBO phases, due to an accelerated deep branch of the BDC and intensified tropical upwelling. However, the MW-induced subseasonal temperature variability in the TTL is modulated by the QBO-dependent zero wind line and, consequently, extends to lower levels in the eQBO than in the wQBO winters (see gray contours in Figures 3b1 and 3b2). When an MW happens in a wQBO winter, temperature variations occur mainly above 440 K and do not significantly influence the stratospheric water vapor entry values. However, in an eQBO winter, the tropical response from the shallow branch of the BDC occurs at lower altitudes, close to the tropopause and thus more likely drives an extradehydration at the tropical tropopause 10–30 days after the MW event.

4. Discussion

A clear dehydration of air entering the tropical stratosphere was diagnosed after MWs. The related tape recorder pattern starts at the tropical tropopause and propagates upward in both QBO phases during the following 2–3 months. The enhanced breaking of planetary waves in the subtropics during eQBO phase results in a distinct cooling and a subsequent drying at the tropical tropopause by ~0.3 ppmv around 3 weeks after the MW. In the wQBO phase this drying effect is also present but smaller and more uniformly distributed over time. Moreover, the MW-induced tropical upwelling is stronger in the eQBO than in the wQBO phase and results in a faster upward transport of the dehydrated air masses.

Since the sharp and unexpected drop (~0.4 ppmv) in stratospheric water vapor after 2000 was documented [*Randel et al.*, 2006], a number of studies tried to explain this drop in different aspects: drop of tropical temperature in relation to increased BDC [*Randel et al.*, 2006; *Bönisch et al.*, 2011] and sea surface temperature (SST) increases in the tropical warm pool [*Rosenlof and Reid*, 2008]. In our study, an extradehydration in relation to MW was clearly diagnosed, combining a decadal variability in the frequency of MWs: 11 events in the 2000s but only 1 event in the 1990s. In addition, extradehydration due to MWs (less inmixing from higher latitudes due to faster upwelling), can last longer than 4 months although the MW itself is confined to boreal winter. Therefore, we looked into 10 year period differences of H_2O anomalies in Figure 4 and found a similarity of H_2O decadal difference and MW-associated drying effect (Figure 3). The similar pattern in H_2O differences between 1980s (8 MWs) and 1990s (1 MW) further supports the following hypothesis (more details in the supplement): the MW-associated drying effect possibly has a contribution to the long-term variability of stratospheric H_2O. The quantification of various contributions to variability of stratospheric H_2O needs further investigation (e.g., the full dynamic control simulation without MWs).

Acknowledgments
We thank ECMWF for providing meteorological reanalysis data. These data are free available from the ECMWF WEB page: http://data-portal.ecmwf.int/data/d/interim_daily/. We thank MLS and HALOE team for providing the H_2O data. The MLS data are available at http://mirador.gsfc.nasa.gov. HALOE data were downloaded from http://haloe.gats-inc.com/home/index.php. The CLaMS model data may be requested from the corresponding author (m.tao@fz.juelich.de).

The Editor thanks two anonymous reviewers for their assistance in evaluating this paper.

References

Andrews, D. G., J. R. Holton, and C. B. Leovy (1987), *Middle Atmosphere Dynamics*, Academic Press, San Diego, Calif.
Baldwin, M. P., et al. (2001), The quasi-biennial oscillation, *Rev. Geophys.*, *39*(2), 179–229.
Bönisch, H., A. Engel, T. Birner, P. Hoor, D. W. Tarasick, and E. A. Ray (2011), On the structural changes in the Brewer-Dobson circulation after 2000, *Atmos. Chem. Phys.*, *11*(8), 3937–3948.

Brewer, A. W. (1949), Evidence for a world circulation provided by the measurements of helium and water vapour distribution in the stratosphere, *Q. J. R. Meteorolog. Soc.*, *75*, 351–363.
Calvo, N., R. Garcia, W. Randel, and D. Marsh (2010), Dynamical mechanism for the increase in tropical upwelling in the lowermost tropical stratosphere during warm ENSO events, *J. Atmos. Sci.*, *67*(7), 2331–2340.
Charlton, A. J., and L. M. Polvani (2007), A new look at stratospheric sudden warmings. Part I: Climatology and modeling benchmarks, *J. Clim.*, *20*(3), 449–469.
Chen, G., and L. Sun (2011), Mechanisms of the tropical upwelling branch of the Brewer-Dobson circulation: The role of extratropical waves, *J. Atmos. Sci.*, *68*, 2878–2892.
Dee, D. P., et al. (2011), The ERA-Interim reanalysis: Configuration and performance of the data assimilation system, *Q. J. R. Meteorolog. Soc.*, *137*, 553–597, doi:10.1002/qj.828.
Dessler, A., M. Schoeberl, T. Wang, S. Davis, and K. Rosenlof (2013), Stratospheric water vapor feedback, *Proc. Natl. Acad. Sci.*, *110*(45), 18,087–18,091.
Fueglistaler, S., and P. H. Haynes (2005), Control of interannual and longer-term variability of stratospheric water vapor, *J. Geophys. Res.*, *110*, D24108, doi:10.1029/2005JD006019.
Fueglistaler, S., et al. (2013), The relation between atmospheric humidity and temperature trends for stratospheric water, *J. Geophys. Res. Atmos.*, *118*, 1052–1074, doi:10.1002/jgrd.50157.
Garcia, R. R., and W. J. Randel (2008), Acceleration of the Brewer-Dobson circulation due to increases in greenhouse gases, *J. Atmos. Sci.*, *65*(8), 2731–2739.
Garny, H., M. Dameris, W. Randel, G. E. Bodeker, and R. Deckert (2011), Dynamically forced increase of tropical upwelling in the lower stratosphere, *J. Atmos. Sci.*, *68*(6), 1214–1233.
Gómez-Escolar, M., N. Calvo, D. Barriopedro, and S. Fueglistaler (2014), Tropical response to stratospheric sudden warmings and its modulation by the QBO, *J. Geophys. Res. Atmos.*, *119*, 7382–7395, doi:10.1002/2013JD020560.
Hegglin, M. I., et al. (2014), Vertical structure of stratospheric water vapour trends derived from merged satellite data, *Nat. Geosci.*, *7*, 768–776, doi:10.1038/NGEO2236.
Hobe, M. V., et al. (2011), Evidence for heterogeneous chlorine activation in the tropical UTLS, *Atmos. Chem. Phys.*, *11*(1), 241–256.
Holton, J. R., P. Haynes, M. E. McIntyre, A. R. Douglass, R. B. Rood, and L. Pfister (1995), Stratosphere-troposphere exchange, *Rev. Geophys.*, *33*, 403–439.
Hurst, D. F., S. J. Oltmans, H. Vömel, K. H. Rosenlof, S. M. Davis, E. A. Ray, E. G. Hall, and A. F. Jordan (2011), Stratospheric water vapor trends over Boulder, Colorado: Analysis of the 30 year Boulder record, *J. Geophys. Res.*, *116*, D02306, doi:10.1029/2010JD015065.
Kerr-Munslow, A., and W. Norton (2006), Tropical wave driving of the annual cycle in tropical tropopause temperatures. Part I: ECMWF analyses, *J. Atmos. Sci.*, *63*(5), 1410–1419.
Konopka, P., et al. (2004), Mixing and ozone loss in the 1999–2000 Arctic vortex: Simulations with the three-dimensional Chemical Lagrangian Model of the Stratosphere (CLaMS), *J. Geophys. Res.*, *109*, D02315, doi:10.1029/2003JD003792.
Kunz, A., R. Müller, V. Homonnai, I. M Jánosi, D. Hurst, A. Rap, P. M Forster, F. Rohrer, N. Spelten, and M. Riese (2013), Extending water vapor trend observations over Boulder into the tropopause region: Trend uncertainties and resulting radiative forcing, *J. Geophys. Res.Atmos.*, *118*, 11,269–11,284, doi:10.1002/jgrd.50831.
Limpasuvan, V., D. Thompson, and D. Hartman (2004), The life cycle of the Northern Hemisphere sudden stratospheric warmings, *J. Clim.*, *17*, 2584–2596.
McKenna, D. S., P. Konopka, J.-U. Grooß, G. Günther, R. Müller, R. Spang, D. Offermann, and Y. Orsolini (2002), A new Chemical Lagrangian Model of the Stratosphere (CLaMS): 1. Formulation of advection and mixing, *J. Geophys. Res.*, *107*(D16), 4309, doi:10.1029/2000JD000114.
Mote, P. W., K. H. Rosenlof, M. E. McIntyre, E. S. Carr, J. G. Gille, J. R. Holton, J. S. Kinnersley, H. C. Pumphrey, J. M. Russell III, and J. W. Waters (1996), An atmospheric tape recorder: The imprint of tropical tropopause temperatures on stratospheric water vapor, *J. Geophys. Res.*, *101*, 3989–4006.
Mote, P. W., T. J. Dunkerton, M. E. McIntyre, E. A. Ray, P. H. Haynes, and J. M. Russell III (1998), Vertical velocity, vertical diffusion, and dilution by midlatitude air in the tropical lower stratosphere, *J. Geophys. Res.*, *103*, 8651–8666.
Norton, W. (2006), Tropical wave driving of the annual cycle in tropical tropopause temperatures. Part II: Model results, *J. Atmos. Sci.*, *63*(5), 1420–1431.
Oltmans, S. J., H. Vömel, D. J. Hofmann, K. H. Rosenlof, and D. Kley (2000), Tropical convective outflow and near surface equivalent potential temperatures, *Geophys. Res. Lett.*, *27*(21), 3453–3456, doi:10.1029/2000GL012133.
Ploeger, F., G. Günther, P. Konopka, S. Fueglistaler, R. Müller, C. Hoppe, A. Kunz, R. Spang, J.-U. Grooß, and M. Riese (2013), Horizontal water vapor transport in the lower stratosphere from subtropics to high latitudes during boreal summer, *J. Geophys. Res. Atmos.*, *118*, 8111–8127, doi:10.1002/jgrd.5063.
Pommrich, R., et al. (2014), Tropical troposphere to stratosphere transport of carbon monoxide and long-lived trace species in the Chemical Lagrangian Model of the Stratosphere (CLaMS), *Geosci. Model Dev.*, *7*(4), 5087–5139, doi:10.5194/gmdd-7-5087-2014.
Randel, W. J., and E. J. Jensen (2013), Physical processes in the tropical tropopause layer and their roles in a changing climate, *Nat. Geosci.*, *6*, 169–176, doi:10.1038/ngeo1733.
Randel, W. J., R. R. Garcia, and F. Wu (2002), Time-dependent upwelling in the tropical lower stratosphere estimated from the zonal-mean momentum budget, *J. Atmos. Sci.*, *59*, 2141–2152.
Randel, W. J., F. Wu, S. J. Oltmans, K. Rosenlof, and G. E. Nodoluha (2004), Interannual changes of stratospheric water vapor and correlations with tropical tropopause temperatures, *J. Atmos. Sci.*, *61*, 2133–2148.
Randel, W. J., F. Wu, H. Vömel, G. E. Nedoluha, and P. Forster (2006), Decreases in stratospheric water vapor after 2001: Links to changes in the tropical tropopause and the Brewer-Dobson circulation, *J. Geophys. Res.*, *111*, D12312, doi:10.1029/2005JD006744.
Riese, M., J.-U. Grooß, T. Feck, and S. Rohs (2006), Long-term changes of hydrogen-containing species in the stratosphere, *J. Atmos. Sol. Terr. Phys.*, *68*(17), 1973–1979.
Rohs, S., C. Schiller, M. Riese, A. Engel, U. Schmidt, T. Wetter, I. Levin, T. Nakazawa, and S. Aoki (2006), Long-term changes of methane and hydrogen in the stratosphere in the period 1978–2003 and their impact on the abundance of stratospheric water vapor, *J. Geophys. Res.*, *111*, D14315, doi:10.1029/2005JD006877.
Rosenlof, K., et al. (2001), Stratospheric water vapor increases over the past half-century, *Geophys. Res. Lett.*, *28*(7), 1195–1198.
Rosenlof, K. H., and G. C. Reid (2008), Trends in the temperature and water vapor content of the tropical lower stratosphere: Sea surface connection, *J. Geophys. Res.*, *113*, D06107, doi:10.1029/2007JD009109.
Solomon, S., K. Rosenlof, R. Portmann, J. Daniel, S. Davis, T. Sanford, and G.-K. Plattner (2010), Contributions of stratospheric water vapor to decadal changes in the rate of global warming, *Science*, *327*, 1219–1222, doi:10.1126/science.1182488.

Taguchi, M. (2011), Latitudinal extension of cooling and upwelling signals associated with stratospheric sudden warmings, *J. Meteorol. Soc. Jpn.*, *89*(5), 571–580.

Tao, M., P. Konopka, F. Ploeger, J.-U. Grooß, R. Müller, C. Volk, K. Walker, and M. Riese (2015), Impact of the 2009 major stratospheric sudden warming on the composition of the stratosphere, *Atmos. Chem. Phys. Discuss.*, *15*(4), 4383–4426.

Urban, J., S. Lossow, G. Stiller, and W. Read (2014), Another drop in water vapor, *Eos Trans. AGU*, *95*(27), 245–246.